984 *Chem. Mater.* **2011,** *23,* 984–988
DOI:10.1021/cm102657v

CHEMISTRY OF MATERIALS
Article

Epitaxial Strain-Induced Chemical Ordering in $La_{0.5}Sr_{0.5}CoO_{3-\delta}$ Films on $SrTiO_3$

Wolfgang Donner,*[,†] Chonglin Chen,[‡,¶] Ming Liu,[¶] Allan J. Jacobson,[‡,§] Yueh-Lin Lee,[∥] Milind Gadre,[∥] and Dane Morgan[⊥]

[†]*Institut für Materialwissenschaften, Technische Universität Darmstadt, 64287 Darmstadt, Germany,* [‡]*Texas Center for Superconductivity, University of Houston, Houston, Texas 77204, United States,* [¶]*Department of Physics and Astronomy, University of Texas at San Antonio, San Antonio, Texas 78249, United States,* [§]*Department of Chemistry, University of Houston, Houston, Texas 77204, United States,* [∥]*Materials Science Program, University of Wisconsin, Madison, Wisconsin 53706, United States, and* [⊥]*Department of Materials Science and Engineering, University of Wisconsin, Madison, Wisconsin 53706, United States*

Received September 17, 2010. Revised Manuscript Received December 12, 2010

Fast ion conductors are at the foundation of a number of important technologies, ranging from fuel cells to batteries to gas separators. Recent results suggest that strained interfaces and thin films may offer new mechanisms for achieving enhanced ionic transport. In this work, we investigate strained 40-nm films of perovskite $La_{0.5}Sr_{0.5}CoO_{3-\delta}$, which is an important material for solid oxide fuel cell cathodes and oxygen separation membranes. We demonstrate that a strained thin film of $La_{0.5}Sr_{0.5}CoO_{3-\delta}$ on $SrTiO_3$ can have dramatically different anion and cation thermodynamics and kinetics than bulk $La_{0.5}Sr_{0.5}CoO_{3-\delta}$. We use synchrotron X-ray diffraction to show that $La_{0.5}Sr_{0.5}CoO_{3-\delta}$ thin films form an ordered phase at 650 K. The ordered phase consists of La and Sr cations in planes parallel to the surface and is associated with coherent expansion in the *c*-direction of ~5%. This chemical ordering is not observed in the bulk material and is ascribed to the interplay between the epitaxial strain imposed by the substrate, changes in oxygen vacancy content and cation mobility, and the ordering of oxygen vacancies.

Introduction

$La_{0.5}Sr_{0.5}CoO_{3-\delta}$ (LSCO) has been considered as one of the best candidates for cathode materials in solid oxide fuel cells (SOFCs) and for oxygen separating membrane applications.[1] To reduce the working temperature of SOFCs and thereby save costs and enhance the lifetime of the cells, it is necessary to enhance the ion conductivity of the cathode. It has been suggested[2] that one way of enhancing the mobility of oxygen ions is to provide disorder-free channels of oxygen vacancies, using compounds with the perovskite structure that exhibit cation ordering. Although LSCO has otherwise desirable properties, it does not show cation ordering in bulk powder samples.[3,4] Electron microscopy studies on thin films demonstrated the occurrence of superstructures in small regions of the sample, but those have been generally attributed to particular patterns of oxygen vacancy ordering, not to chemical ordering of the cation sublattices.[3] It has been an open question if strain in thin films can be coupled to oxygen partial pressure and temperature control to drive cation and anion ordering in LSCO. Generally, there has been increasing evidence that strain can strongly impact complex oxide thermodynamic and kinetic properties. In particular, in cobaltite films, strain effects associated with different substrates have been implicated in changes in electrical conductivity,[5] spin state,[6] vacancy formation and migration energetics,[7] and oxygen reduction activity.[8] Studies on other oxide conducting systems have also suggested strong coupling of biaxial strain to migration barriers, leading to enhanced diffusion.[9] In this work, we report on the chemical ordering in LSCO films epitaxially grown on [001]-oriented $SrTiO_3$ (STO) and the structure and epitaxy of these films in different oxygen partial pressure environments. We also identify the physical mechanisms by which coupling of strain, defect formation, and migration energetics leads to chemical ordering in LSCO films.

*E-mail: wdonner@tu-darmstadt.de.

(1) Kilner, J. *Solid State Ionics* **2000**, *129*, 13.
(2) Taskin, A.; Lavrov, A.; Ando, Y. *Appl. Phys. Lett.* **2005**, *86*, 091910.
(3) Mizusaki, J.; Mima, Y.; Yamauchi, S.; Fueki, K. *J. Solid State Chem.* **1989**, *80*, 102.
(4) Haggerty, R.; Seshadri, R. *J. Phys.: Condens. Matter* **2004**, *36*, 6477.
(5) Rata, A. D.; Herklotz, A.; Nenkov, K.; Schultz, L.; Doerr, K. *Phys. Rev. Lett.* **2008**, *100*, 076401.
(6) Rondinelli, J. M.; Spaldin, N. A. *Phys. Rev. B* **2009**, *79*, 054409.
(7) Kushima, A.; Yip, S.; Yildiz, B. *Phys. Rev. B* **2010**, *82*, 115435.
(8) la O, G. J.; Ahn, S. J.; Crumlin, E.; Orikasa, Y.; Biegalski, M. D.; Christen, H. M.; Shao-Horn, Y. *Angew. Chem., Int. Ed.* **2010**, *49*, 5344.
(9) Kushima, A.; Yildiz, B. *J. Mater. Chem.* **2010**, *20*, 4809.

 Published on Web 01/12/2011

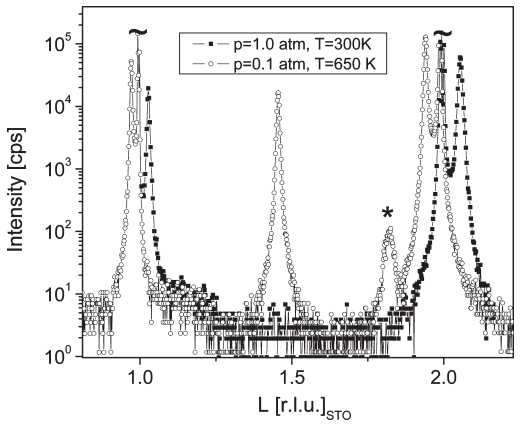

Figure 1. X-ray diffraction (XRD) scans along the surface normal ([00*l*]-direction) of a 40-nm LSCO thin film on STO. Closed symbols represent data obtained in air at a pressure of 1 atm and a temperature of 300 K; open symbols represent data obtained in air at a pressure of 0.1 atm and a temperature of 650 K. Note the large shift of the film peak from the right side of the substrate peak to its left side. The asterisk symbol (∗) denotes a peak from a parasitic phase.

Results and Discussion

Experimental Details. The LSCO thin film was grown on an [001]-oriented STO substrate with a cubic lattice parameter of 0.3905 nm and excellent crystallinity (mosaic spread of < 30 arcsec, miscut angle $< 0.5°$). An LSCO target with dimensions of 1 in. in diameter $\times$ 0.25 in. in thickness was prepared from LSCO powder synthesized by conventional solid-state reaction. The powder was uniaxially pressed and then sintered at 1500 K for 12 h to produce a high-density target. A 248-nm KrF excimer pulsed laser operated at 4 Hz with an energy density of 1.8 J/cm^2 was employed to grow the films by laser ablation. A temperature near 1100 K and a pure oxygen pressure of 300 mTorr were determined to be the optimum deposition conditions. After deposition, the film was annealed at 200 Torr of oxygen for 15 min at a temperature of 1070 K and then cooled to room temperature at a rate of 2.5 K/min in the same oxygen environment.

Bulk LSCO has a pseudo-cubic perovskite structure with lattice parameters, at room temperature, of 0.38337 and 0.38458 nm for samples heated at 1070 K and cooled in air and in UHP argon, corresponding to oxygen atom deficiencies (δ) of 0.09 and 0.21, respectively.

The film structure was characterized by X-ray diffraction (XRD) experiments conducted at the National Synchrotron Light Source in Brookhaven (NY). The *z*-axis diffractometer at beamline X22C was used to carry out in situ experiments inside a mirror furnace equipped with gas flow control and an oxygen sensor. The focused X-ray beam was monochromatized by a Ge(111) double monochromator to a wavelength of 0.11271 nm. Additional structure factor determinations were carried out at the vertical four-circle diffractometer of Beamline X22A operating at a wavelength of 0.11587 nm with the sample at room temperature in air.

Experimental Results. Figure 1 shows a radial scan along the surface normal of a 40-nm as-grown LSCO thin film inside the mirror furnace at 300 K and 1 atm of air (closed symbols); the scan is calibrated in terms of the substrate reciprocal lattice. Only the (00*l*) reflections of LSCO, together with those of STO appear in the diffraction pattern. (The center of the STO reflections is left out of the scan, because of a detector nonlinearity.) This scan illustrates that the LSCO film has its *c*-axis oriented normal to the substrate surface.

The lattice parameter *c*, which is determined from the scan in Figure 1, is 0.3804 nm. After pumping the furnace volume down to 0.1 atm air, no change of the diffraction pattern was detectable within the first hour. Subsequent heating at this pressure first led to a slight lattice parameter change visible at 500 K, but then when the temperature was raised to $T = 650$ K at a heating rate of 1 K/s, a massive change occurred. The open symbols in Figure 1 represent a scan under a steady-state condition of $T = 650$ K. The LSCO(002) reflection had moved from the right side of the STO reflection to its left side ($l = 1.942$). This corresponds to an expansion of the film lattice of 5.7% along the *c*-direction; 0.78% of that value can be attributed to thermal expansion,[10] and the rest results from a structural change described below. At the same time, an additional reflection corresponding to a doubling of the unit cell appeared with a maximum intensity of ~10% of the fundamental (002) reflection. Structure factor calculations show that the intensity of the half-order reflection results not only from an ordering of the oxygen vacancy planes, which would only lead to weak superstructure reflections, but from A-site ordering (i.e., the difference of the form factors of La and Sr).

This enormous lattice expansion is reversible at a temperature of 650 K: venting of the furnace to 1 atm air leads to a shift of the (002) peak back to its original position, together with the disappearance of the half-order reflections. Further heating above $T = 700$ K leads to a morphological change of the film and finally to dewetting at 1000 K. An additional small (0.1%) reflection also appears after the first expansion of the lattice at a value of $l = 1.82$ (asterisk). This parasitic reflection has a rocking width of several degrees and thereby does not belong to the main structural phase of the lattice nor the superstructure.

Figure 2 is a grazing-incidence XRD scan along the [*h*00] direction of the substrate at an incident angle, resulting in a scattering depth of 50 nm. One sharp LSCO(200) reflection is visible, together with the STO-(200) reflection; the two reflections differ in their transverse (rocking) width. This type of scan appears identical for films that are vertically expanded (oxygen-deficient) and for oxygen-loaded films. From the position of the peak, we calculate a lattice parameter *a* of 0.3868 nm; a comparison to the 0.3905 nm value for the STO substrate shows a partial relaxation of the epitaxial strain. A complete analysis leads to an interfacial relation of LSCO(001)//STO(001) and LSCO[100]//STO[100]. The inset of Figure 2 shows an overview of other reflections detected in the *h*0*l*-plane using four-circle diffractometry.

(10) Ullmann, H. *Solid State Ionics* **2000**, *138*, 79.

The two scans of Figures 1 and 2 are marked as arrows in the reciprocal lattice sketch. We find that the primitive tetragonal symmetry of space group $P4/mmm$ is compatible with our observations. Only one tetragonal domain, with its long axis parallel to the surface normal, could be detected, leaving the reflections of other possible domains absent. An additional, small parasitic reflection can be detected at $h = 1.827$ (asterisk). Together with other reflections (see above), we conclude that the parasitic phase has face-centered cubic (fcc) symmetry; most likely, it is SrO, with a volume fraction of $< 1\%$.

We derived the structural models of Figure 3 from the intensities of the observed film reflections in the pseudocubic and the expanded, tetragonal phase. Other oxygen vacancy superstructures without A-site ordering can be excluded, since the observed intensities in the half-order reflections are too high to be induced by vacancy ordering alone. The left inset shows two unit cells of the pseudocubic phase with the La and Sr cations randomly distributed. The Co ions are octahedrally coordinated by O ions and each O ion is shared by two Co ions. Heating the sample under a lower oxygen partial pressure leads to the removal of the apical oxygen (one out of six oxygen atoms), together with the chemical ordering of the cations. La^{3+} (small spheres) ions move into the oxygen-deficient planes, whereas Sr^{2+} ions (large spheres) are located within the oxygen-containing planes (right structure). The intensities of the half-order reflection cannot be explained with oxygen vacancy ordering alone, but require cation ordering to be taken into account. In the particular example shown above, the degree of chemical ordering within the cation sublattices is ~66%. This value of the order parameter can be derived from the relative intensities of fundamental and superstructure (half-order) reflections and implies that 17% of the La (and Sr) atoms are on the "wrong" site (the order parameter has a value of zero at 50% La occupation and one at 100%). The cobalt coordination changes to square-pyramidal, leaving the Co ion in a mixed-valence state (oxidation state of 2.5), slightly lifted from the pyramid base (our best-fit value is $z = 0.23$). The size difference between the La^{3+} (1.16 Å (VIII)) and Sr^{2+} (1.44 Å (XII)) ions, together with the Coulomb repulsion between the Co ions leads to the huge lattice expansion of 5.7%. Because of the epitaxial clamping effect, the a and b lattice parameters remain unchanged. Note that this type of ordering, with the oxygen vacancies and the smaller trivalent (3+) cation primarily in one cation plane and the oxygen and larger divalent (2+) cation primarily in the other cation plane, has been widely observed in similar systems (e.g., in the structure of $(GdBa)CoO_3$,[2] $(PrBa)CoO_3$,[11] and $YSr_2Cu_2FeO_{7.53}$[12]). A comparison of the ab initio energy of the structure in Figure 3 with swapped La and Sr layers (i.e., with the Sr in the plane with oxygen vacancies) shows that the proposed ordering is more stable, by ~210 meV/formula unit. Ceramic $La_{0.5}Sr_{0.5}CoO_{3-\delta}$ powder samples are known to exhibit a lattice expansion upon oxygen removal.[3,4] However, this expansion is not larger than 0.34% at $\delta = 0.21$. Under the conditions used in this experiment (650 K, 0.1 atm), bulk LSCO would show an oxygen stoichiometry of $\delta < 0.1$.[3] We estimate the oxygen stoichiometry to be $\delta = 0.5$, based

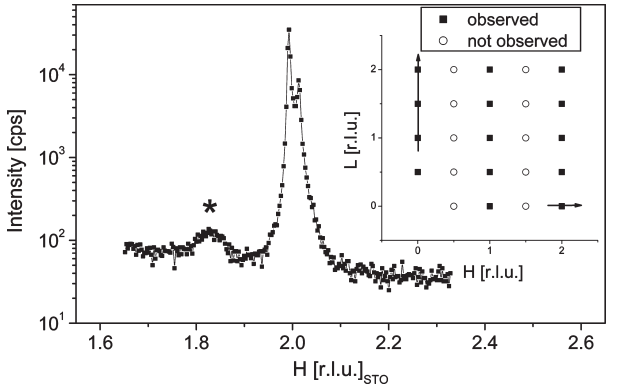

Figure 2. Grazing-incidence XRD along the [h00] direction of LSCO/STO. The inset shows the reciprocal $h0l$-plane of the film, together with the direction of the scan performed in this figure (denoted by a horizontal arrow) and in Figure 1 (denoted by a vertical arrow).

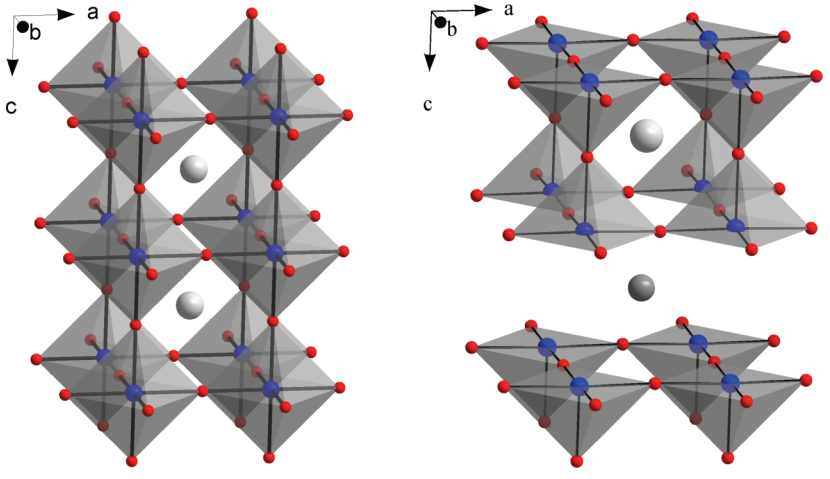

Figure 3. (Left) Model of the structure of LSCO under ambient conditions; displayed are two unit cells with the Co ions located inside the oxygen octahedrons. Large spheres represent La and Sr cations randomly distributed on the center sites. (Right) Model of the structure of the cation-ordered phase; the apical oxygen site is vacated and the unit cell is doubled. Large spheres represent Sr atoms, and small spheres La atoms. The La and Sr are pictured as being perfectly ordered, but significant disorder still exists between the La and Sr layers.

Table 1. Ab Initio La^{3+} A-Site Vacancy Hopping Barrier (E_{mig}) vs Strain in $LaCoO_3$ and the Relative Energy of the Ordered Compound (Given in Figure 1) and a Disordered Phase (Represented by 2 × 2 × 2 Perovskite Supercell Special Quasirandom Structures (SQS)[21] of Sr and O Vacancies) at Composition $La_{0.5}Sr_{0.5}CoO_{2.5}$[a]

	E_{mig}(eV)		
strain (%)	optimal c	5% increase of c	$\Delta E_{ordering}$ (eV/Co)
0	3.38		0.14 ± 0.05
1.9	2.68	1.29	0.13 ± 0.03
4	2.45		

[a] Error bars are based on the standard deviation in the mean of the two SQS energy values.

on the lattice expansion measured in our films and the observed structure factors. In addition, no cation ordering (doubling of the unit cell) is observed in bulk LSCO. We conclude that the strain imposed by the epitaxial growth on STO imposes a boundary condition that makes it energetically favorable for the La and Sr to order into different planes.

Ab Initio Theory Results. In the above model, we have made three implicit assumptions about differences between thin film and bulk LSCO thermokinetic properties. Here, we validate these assumptions using density function theory (DFT)-based ab initio methods. All calculations are done with GGA+U[13] in the spherically averaged approximation[14] ($U - J = 3.3$ eV[15,16]), using the VASP code.[17,18] Some calculations have been done on $LaCoO_3$ (LCO) or $La_{0.875}Sr_{0.125}CoO_{3-\delta}$ to reduce the complexity associated with different Sr arrangements, but we expect the trends to also apply to $La_{0.5}Sr_{0.5}CoO_{3-\delta}$.

The first property change implicit in our model is that, for the observed behavior to occur, there must be cation hopping at 650 K in the film. To obtain cation motion on the time scale of the experiment, we require a hopping rate of approximately one hop per second. If we assume a hopping rate of $r = 5 \times 10^{12} \exp[-E_{mig}/(kT)]$, then obtaining a rate of approximately one hop per second requires a migration barrier of $E_{mig} \approx 1.6$ eV. This estimated migration barrier is far smaller than typical bulk A-site perovskite cation migration barriers, which are ~3−4 eV.[19,20] However, Table 1 shows that the ab-initio-predicted La migration barrier in $LaCoO_3$ is dramatically reduced by both the epitaxial strain and c-lattice expansion. The barriers were determined by elastic band calculations in a $2\sqrt{2} \times 2\sqrt{2} \times 2$ perovskite supercell with a single A-site cation vacancy and three additional electrons added to maintain the Co^{3+} valence. The scale of the changes in barriers associated with strain and c-lattice expansion are large enough to allow for cation mobility in a $La_{0.5}Sr_{0.5}CoO_{3-\delta}$ thin film at 650 K.

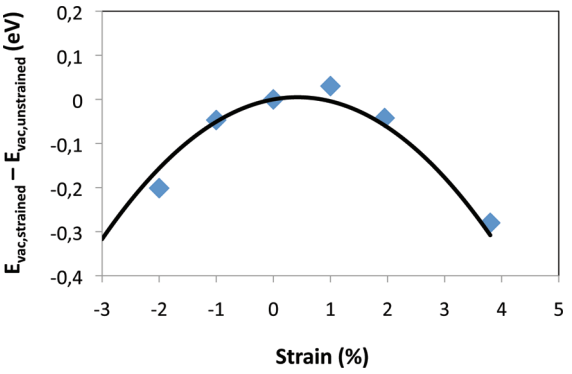

Figure 4. Ab initio oxygen vacancy formation energy (E_{vac}) versus strain for $La_{0.875}Sr_{0.125}CoO_{3-\delta}$. The solid line denotes data from a simple model that includes only chemical-induced changes in elasticity and lattice parameter (see text).

The second property change implicit in the model is that vacancy formation for $La_{0.5}Sr_{0.5}CoO_{3-\delta}$ must be easier in the thin film than in the bulk. Under the given experimental conditions ($T = 650$ K, $p(O_2) = 0.1$ atm), we can take $\delta = 0.1$[4] as the upper bound for the vacancy content in the bulk phase. However, the vacancy concentration of our film is $\delta \approx 0.5$. Based on the Lankhorst model[22] for LSC, an increase in the observed vacancy concentration from $\delta = 0.1$ to $\delta = 0.5$ corresponds to a vacancy formation energy reduction (making it easier to form vacancies) of ~0.1 eV in the film, compared to that in the bulk.

Figure 4 shows that the ab initio calculated vacancy formation energy of $La_{0.875}Sr_{0.125}CoO_{3-\delta}$ generally decreases significantly from the unstrained bulk value with increasing or decreasing strain. In this calculation, δ changes from 0.0625 to 0.125 in forming the vacancy and the $\delta = 0.125$ calculation consists of a $2\sqrt{2} \times 2\sqrt{2} \times 2$ perovskite supercell with two maximally separated Sr cations, each with first-neighbor vacancies. The ab initio result predicts a reduction of more than 0.05 eV, relative to the unstrained bulk for the observed +1.95% strain in the films measured here, which is consistent with the reduction between bulk and strained film of ~0.1 eV estimated from the experimental data. The strain dependence observed here is in qualitative agreement with the trend of reduced vacancy formation energy observed in the ab initio studies of Kushima et al.[7] on $LaCoO_3$ (LCO) under tensile strain up to 0.02. However, the changes in vacancy formation energy with strain in their LCO data are far more extreme than that found in the LSCO studies presented here. The source of this discrepancy is not clear but perhaps reflects the complex alterations in electronic structure that occur with Sr doping. Our calculated strain dependence of the vacancy formation energy for films can be understood in terms of a simple elasticity and

(11) Kim, G.; Wang, s.; Jacobson, A. J.; Reimus, L.; Brodersen, P.; Mims, C. A. *J. Mater. Chem.* **2007**, *17*, 2500.
(12) Slater, P. R.; Greaves, C. *Physica C* **1991**, *180*, 299.
(13) Anisimov, V. I.; Aryasetiawan, F.; Lichtenstein, A. I. *J. Phys.: Condens. Matter* **1997**, *9*, 767.
(14) Dudarev, S. L.; Botton, G. A.; Savrasov, S. Y.; Humphreys, C. J.; Sutton, A. P. *Phys. Rev. B* **1998**, *57*, 1505.
(15) Wang, L.; Maxisch, T.; Ceder, G. *Phys. Rev. B* **2006**, *73*, 195107.
(16) Lee, Y.-L.; Kleis, J.; Rossmeisl, J.; Morgan, D. *Phys. Rev. B* **2009**, *80*, 224101.
(17) Kresse, G.; Hafner, J. *Phys. Rev. B* **1993**, *47*, 558.
(18) Kresse, G.; Furthmuller *Phys. Rev. B* **1996**, *54*, 1169.
(19) Souza, R. A. D.; Islam, M. S.; Ivers-Tiffee, E. *J. Mater. Chem.* **1999**, *9*, 1621.
(20) Jones, A.; Islam, M. S. *J. Phys. Chem. C* **2008**, *112*, 4455.
(21) Zunger, A.; Wei, S. H.; Ferreira, L. G.; Bernard, J. E. *Phys. Rev. Lett.* **1990**, *65*, 353.
(22) Lankhorst, M. H. R.; Bouwmeester, H. J. M.; Verweij, H. *Phys. Rev. Lett.* **1996**, *77*, 2989.

formation volume model. Specifically, we observe a decreasing value of the Young's modulus with increasing vacancy content, as well as small changes in equilibrium volume, because of chemical expansion.[23] For example, our calculated Young's modulus changes from 186 GPa to 164 GPa for an oxygen stoichiometry of $\delta = 0.0625$ and 0.125, respectively. This decrease of Young's modulus with increasing vacancy content is consistent with measurements in $La_{0.8}Ca_{0.2}CoO_3$ and $La_{0.8}Sr_{0.2}CoO_3$,[1,24,25] although the calculated values are 5%−18% higher than experimental values.[26] The trend of Young's modulus with vacancy content implies that films with more vacancies can be strained more easily, or equivalently, that strained films form vacancies more easily. We also predict a chemical expansivity of 0.113 for $LaCoO_{3-\delta}$ at $\delta = 0.125$, which is consistent with the value of 0.129 for $La_{0.6}Sr_{0.4}CoO_3$ and 0.112 for $La_{0.8}Sr_{0.2}CoO_3$ measured by Chen et al.[27] Predicting the vacancy formation energy versus strain from just the calculated Young's moduli changes and shifts in equilibrium volume gives the solid curve in Figure 4. The excellent fit between the model and the direct ab initio calculation demonstrates that the changes in Young's modulus and volume with vacancy content are adequate to model the data. The slight shift to the right of the peak in the curve is due to the negative vacancy formation volume favoring compression in the more-defected phase, an effect which causes the vacancy formation energy to increase slightly with small amounts of positive strain.

The third property implicit in the model is that the ordered phase is more stable than the solid solution at 650 K, at least for the thin film. If the ordered phase is more stable in both the bulk and the film, then it must be explained why the ordered phase is able to form in the thin film and not in the bulk. Table 1 shows the ab initio predicted relative energy of the ordered compound identified in this work (given in Figure 3) and a disordered phase (represented by $2 \times 2 \times 2$ perovskite supercell SQS[21] of Sr and O vacancies) at composition $La_{0.5}Sr_{0.5}CoO_{2.5}$. Note that the calculated ordered phase is quite idealized, with perfect ordering of La and Sr layers as in Figure 3, and it does not contain the partial cation disorder identified experimentally above. Therefore, this ordered phase should not be taken as the most stable ordered structure but merely as a qualitative guide to the trends in ordering energy. For both the bulk and strained structure, the ordered compound is significantly more stable than the disordered phase. The stabilization energy is $\sim 140 \pm 50$ meV/Co (this result is averaged over two SQS), which is approximately $(2-3)kT$ at $T = 650$ K and, therefore, an energy scale consistent with ordering in the range of 650 K. Interestingly, the ab initio results suggest that the strain has a small effect on ordering tendency, which would imply that the ordered phase could also form in the bulk. Therefore, the presence of ordering in the film and not the bulk is likely due to the larger concentration of vacancies (which can drive the ordering) and the increased kinetics at lower temperatures of the film, compared to the bulk. The ordered phase that we calculated shows a *c*-expansion of 1%, compared to the SQS, which is not as large as that seen in the experiments. The origin of this discrepancy is not clear but may be due to the fact that we have not identified the exact ordered compound obtained in the films (e.g., the experiments show partial ordering of cations, whereas our model assumes perfect ordering) or to GGA errors in the subtle interplanar interactions necessary to obtain an accurate *c*-lattice expansion.

Conclusions

In conclusion, we have observed a structural phase transition in $La_{0.5}Sr_{0.5}CoO_{3-\delta}$ (LSCO) thin films, as a function of oxygen partial pressure. La and Sr cations, as well as oxygen vacancies, show ordering under reducing conditions at elevated temperatures. The transition is reversible and most likely induced by epitaxial strain imposed by the $SrTiO_3$ (STO) substrate. Ab initio calculations suggest that the strain does not strongly alter the intrinsic ordering tendencies but instead enhances both vacancy concentration (through lower vacancy formation energy) and cation mobility, enabling the ordered phase to form at $T = 650$ K. The present structure is not practical for most applications, because STO is not a good ion conductor. However, other ion-conducting substrates (e.g., lanthanum strontium gallate magnesite (LSGM), etc.) could potentially provide the desired ionic conductivity and still provide the necessary strain to enhance the LSCO properties. This work provides a foundation for additional studies of the strained LSCO, to determine if cation ordering enhances the ionic conductivity as seen in Taskin et al.[2]

Acknowledgment. This work was supported by the National Science Foundation (under DMR Grant No. 0502740) and the U.S. Department of Energy (U.S. DOE), Office of Basic Energy Sciences, Division of Materials Sciences and Engineering (under Award No. DE-SC0001284) (theoretical studies). Research carried out at the NSLS, BNL, was supported by the U.S. DOE, Division of Material Sciences and Division of Chemical Sciences (under Contract No. DE-AC02-98CH10886). Financial support for the work at the University of Wisconsin, from the National Science Foundation MRSEC program (under Grant No. DMR-0520527) and computing support from NERSC allocation of the Center for Nanophase Materials Sciences (CNMS) at Oak Ridge National Laboratory (under Grant No. CNMS2008-204) also are gratefully acknowledged.

(23) Duncan, K. L.; Wang, Y. L.; Bishop, S. R.; Ebrahimi, F.; Wachsman, E. D. *J. Am. Chem. Soc.* **2006**, *89*, 3162.
(24) Orlovskaya, N.; Kleveland, K.; Grande, T.; Einarsrud, M. A. *J. Eur. Ceram. Soc.* **2000**, *20*, 51.
(25) Orlovskaya, N.; Lugovy, M.; Pathak, S.; Steinmetz, D.; Lloyd, J.; Fegely, L.; Radovic, M.; Payzant, E. A.; Lara-Curzio, E.; Allard, L. F.; Kuebler, J. *J. Power Sources* **2008**, *182*, 230.
(26) Lengsdorf, R.; Ait-Tahar, M.; Saxena, S. S.; Ellerby, M.; Khomskii, D. I.; Micklitz, H.; Lorenz, T.; Abd-Elmeguid, M. M. *Phys. Rev. B* **2004**, *69*, 140403.
(27) Chen, X. Y.; Yu, J. S.; Adler, S. B. *Chem. Mater.* **2005**, *17*, 4537.